JOURNAL OF Materials CHEMISTRY

A shift-lattice description of some face centred cubic alloy superstructures

Part 1.—One-dimensional structures†

Richard J. D. Tilley[a] **and R. Phillip Williams**[b]

[a]*School of Engineering and* [b]*Department of Physics, University of Cardiff, PO Box 685, Cardiff, UK CF2 3TA*

Both metal atom components of a number of binary alloy structures, mainly occurring in the Au-rich region of the Au–Mn system, have been analysed as shift-lattices. It is shown that both atom types lie upon separate complementary shift-lattices. All the structures can be reproduced by a smooth variation of the shift-lattice parameters. Those found experimentally form only a small set of the infinite family of commensurate and incommensurate structures which can be constructed *via* the shift-lattice method. The diffraction patterns of these phases can readily be derived and the relationship of the diffraction patterns observed to the separate components from each of the contributing shift-lattices is described.

Introduction

The shift-lattice formalism has been used to unify information about the crystal structures and diffraction patterns of a wide range of non-stoichiometric compounds.[1–3] The method is applicable to the many materials which can be described, in one form or another, as containing fragments of one lattice type embedded within another. Previous studies have focused upon crystallographic shear structures,[4,5] the niobium oxide block structures[6] and several alloy structures.[7]

In a recent paper the structures of a disparate group of Au–Mn alloys with compositions near to Au_4Mn were shown to be easily related to each other *via* shift-lattice distributions of fragments of Au_4Mn structure in a face centred cubic (fcc) matrix of Au atoms.[8] However, not all aspects of these phases were clarified. In particular it was thought desirable to determine if both the Au and Mn components of these shift-lattice structures were themselves distributed as separate shift-lattices. In addition, the relationship between the diffraction patterns of each of the components in the structure and the overall diffraction patterns, which clearly displayed shift-lattice characteristics, was not determined. In this paper we consider, for the first time, the shift-lattice aspects of both components in these and related alloy structures and clarify the problem of the diffraction patterns mentioned above.

Shift-lattice terminology

The shift-lattice[1–8] is a method of distributing and analysing structures made up of recognisable fragments of a lattice. One-dimensional shift-lattices are made up of slabs which generally possess small (or 'normal') lattice parameters in two directions but a long lattice parameter in the third. It is repetition in this long direction that concerns us in this paper. There are a number of points of terminology which apply to the rest of the paper and which are collected here to save repetition.

The fundamental unit of interest in this paper is a lattice (which in this case is related to the Au_4Mn structure). The lattice is described by three lattice vectors together with the angles between them as in normal crystallographic usage. In the one-dimensional case only two lattice vectors are needed. Extended structures are built up of fragments of this lattice. These fragments are delineated in extent by *g*-functions of width *w*, which are defined by the knowledge that the lattice exists within the *g*-functions but not outside it. There is some ambiguity about points which lie exactly on the boundary but this can be resolved in real cases by a decision as to whether they should be included within the *g*-function or not. In the one-dimensional case the *g*-function boundaries are represented by continuous lines which are infinitely long and the lattice by the important lattice vectors α_1 and α_2.

The complete lattice (or structure) is built up from identical lattice fragments, identically oriented and contained in identical *g*-functions. The separation of the *g*-functions is designated β. The *g*-functions can be separated, which occurs when β is greater than *w*, or overlapping when β is less than *w*. This arrangement will, to a large extent, be governed by the geometry of the real structures under consideration. A key feature of the construction is that the lattice fragment in each *g*-function is displaced from that in neighbouring *g*-functions by a shift of ε, where ε can be any number whatsoever (*i.e.* not necessarily an integer), but is most conveniently expressed in terms of α. These points will be illustrated in the figures below.

The structure of Au_4Mn

Au_4Mn crystallises in the tetragonal Ni_4Mo structure, shown in Fig. 1(*a*), with lattice parameters $a = 0.645$ nm, $c = 0.403$ nm.[9] It is seen to be a superstructure of the fcc Au structure. In our previous paper[8] the Mn distribution in Au_4Mn was taken as the parent motif from which the Mn distributions in all the other known Au–Mn alloy structures could be derived *via* application of the shift-lattice construction. This starting point is not unique and a number of different shift-lattice descriptions of the same structures can be employed, in the same way that a number of different unit cells can be defined for any one crystal structure. In this paper, because we wish to consider both atomic components of the structure separately, it becomes convenient to subdivide the crystal into Au-only and Mn-only regions. One way of achieving this for Au_4Mn is shown in Fig. 1(*b*).

An examination of Fig. 1 confirms that both the Au and Mn portions of the structure are shift-lattices. The shift-lattice formalism has been described in detail elsewhere[1–3] and here just those aspects of terminology will be introduced for the immediate purpose. The basic lattice used in this paper is defined by two vectors α_1 and α_2 defined with respect to the

† Presented at the RSC Autumn Meeting, 2–5 September 1997, University of Aberdeen, Scotland.

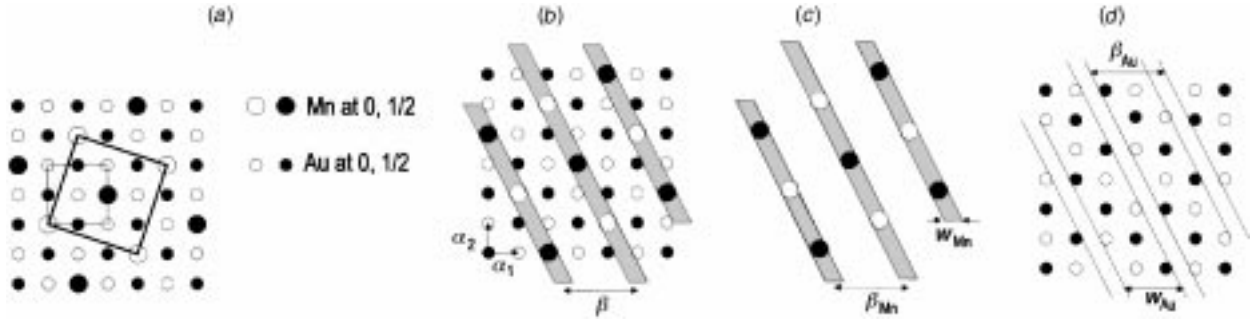

Fig. 1 (*a*) The Au_4Mn structure. The heavy outline shows the unit cell, and the light outline shows the fcc subcell. (*b*)–(*d*) A shift lattice description of Au_4Mn. The slanting lines are the *g*-function boundaries, which are coincident for the Mn (*c*) and Au (*d*) portions of the structure. The Mn-containing *g*-functions are shaded. The shift-lattice parameters α_1, α_2 and w_{Mn}, w_{Au}, and β are indicated.

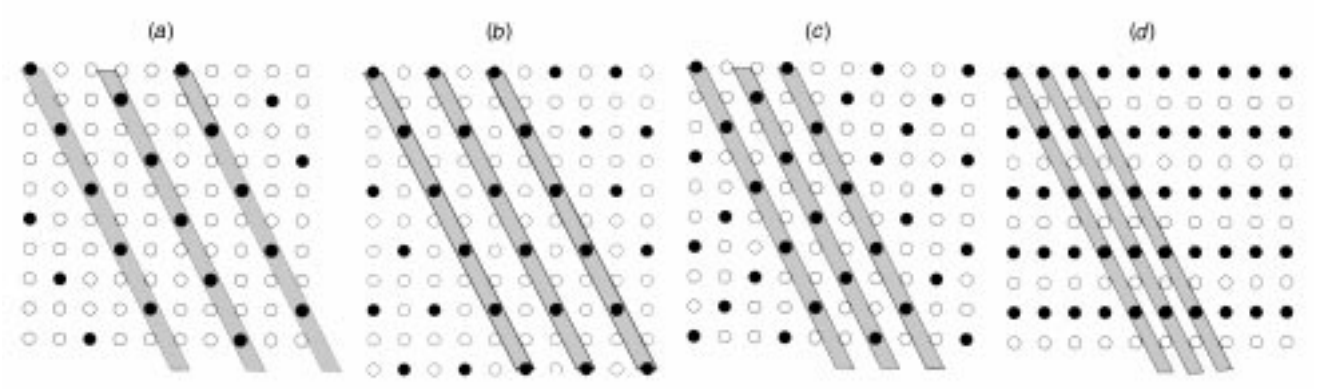

Fig. 2 (*a*) Projections of the structures of (*a*) Au_4Mn, (*b*) Al_3Ti, (*c*) Pt_2Mo and (*d*) CuAu I. In each diagram the Mn atoms are shown as filled circles and the Au atoms as open circles; *g*-function boundaries are shown as slanting lines and the Mn-containing *g*-functions are shaded. They are coincident for both the Mn and Au portions of the structure. For clarity not all of the *g*-function boundaries are drawn and the atom heights are not indicated.

fcc sublattice as shown in Fig. 1(*b*). The regions in which a lattice exists are defined by a *g*-function. The *g*-function boundaries which delineate the two shift-lattices, drawn as lines in Fig. 1(*b*), are coincident and lie on (210) planes with respect to the fcc subcell. The width of each *g*-function is defined as w_{Mn} and w_{Au} respectively. The two separate shift-lattices are drawn in Fig. 1(*c*), (*d*). Because the atoms are all positioned upon the nodes of the basic α_1–α_2 square lattice, shown in Fig. 1(*b*), the form is especially simple as the shifts ε_1 parallel to α_1 and ε_2 parallel to α_2, are zero. It is also apparent from Fig. 1 that the values of the shift-lattice parameters β_{Au} and β_{Mn}, which define the separations of the *g*-functions of each component lattice, are the same for each shift-lattice. This is also so in the other structures described in this paper and the parameter will simply be referred to as β. The shift lattice parameters for the Au and Mn components of Au_4Mn are summarised in Table 1.

Table 1 Shift lattice parameters for the Au_4Mn (210) homologous series of structures

formula	atom type	w	β
A_6B	B	$0.5\alpha_1$	$3.5\alpha_1$
	A	$3.0\alpha_1$	$3.5\alpha_1$
A_5B	B	$0.5\alpha_1$	$3.0\alpha_1$
	A	$2.5\alpha_1$	$3.0\alpha_1$
Au_4Mn	Mn	$0.5\alpha_1$	$2.5\alpha_1$
	Au	$2.0\alpha_1$	$2.5\alpha_1$
Al_3Ti	Ti	$0.5\alpha_1$	$2.0\alpha_1$
	Al	$1.5\alpha_1$	$2.0\alpha_1$
Pt_2Mo	Mo	$0.5\alpha_1$	$1.5\alpha_1$
	Pt	$1.0\alpha_1$	$1.5\alpha_1$
AuCu	Au	$0.5\alpha_1$	$1.0\alpha_1$
	Cu	$0.5\alpha_1$	$1.0\alpha_1$

The (210)-derived family of one-dimensional shift-lattice structures

A vast number of structures similar to Au_4Mn can be constructed by varying the parameters of these two shift-lattices while ensuring that the geometry of the final structure is compatible with the fcc sub-structure. Here and in the rest of this paper only structures in which the Mn-containing *g*-functions are approximately one atom wide are considered, as in the structure of Au_4Mn. To illustrate some of these, Fig. 2 shows members of the homologous series Au_nMn. [In these and subsequent figures the heights of the Au and Mn atoms will be ignored and the two atoms differentiated by open (Au) and filled (Mn) circles. In addition, only some *g*-function boundaries are drawn.] The phases can be constructed from Au_4Mn by varying the only independent parameter, β, as w_{Mn} is fixed and w_{Au} is given by $\beta - w_{Mn}$. The shift-lattice parameters for these structures are given in Table 1. In each structure (as in all of the subsequent structures in this paper) both the Au

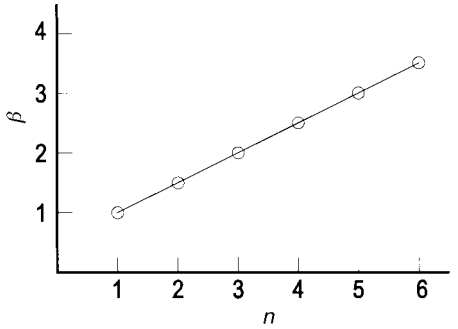

Fig. 3 A graph of β *vs.* the value of n in the series formula A_nB

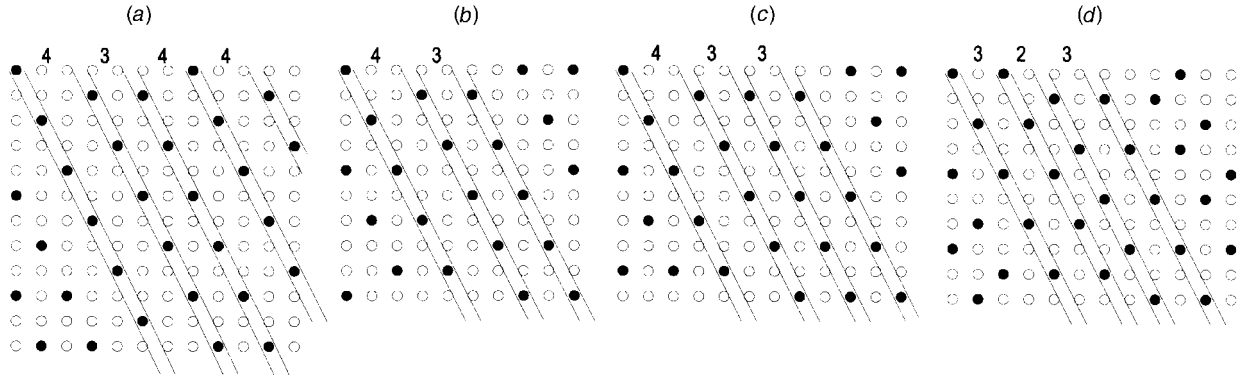

Fig. 4 The structures of (*a*) $Au_{22}Mn_6$, (*b*) A_7B_2, (*c*) $A_{10}B_3$ and (*d*) Al_8Mo_3. The *g*-function boundaries are shown as sloping lines and the width of the adjoining slabs are shown above the Au portions.

and Mn atoms form shift-lattices. The *g*-functions, shown by lines, are adjacent and on (210) planes.

None of these structures are found in the Au–Mn system, but do occur in other alloys. The $n=3$ structure is that of Al_3Ti,[10] the $n=2$ structure is that of Pt_2Mo[11] and the $n=1$ structure that of CuAu.[9]

A plot of the key parameter β *versus* the value of n in Au_nMn is given in Fig. 3. There is no reason for restricting the value of β to those half-integral values needed to generate the homologues just described. Choosing values of β between those used in constructing the phases shown in Fig. 2 while keeping the *g*-function boundaries on (210) planes will produce 'ordered intergrowths' of the two parent structures on either side. Some of this multitude of structures are shown in Fig. 4.

For a value of β equal to $2.333\alpha_1$ the $Au_{22}Mn_6$[12] structure, shown in Fig. 4(*a*), is produced. This structure can be described as an 'ordered intergrowth' of two slabs of the higher parent structure Au_4Mn interleaved with one slab of the lower parent structure (Au_3Mn) with the Al_3Ti structure. If this phase is designated as (443) then a slight decrease in β to $2.25\alpha_1$ yields the (43) structure of hypothetical Au_7Mn_2, shown in Fig. 4(*b*). A further decrease of β to $2.166\alpha_1$ produces the hypothetical phase $Au_{10}Mn_3$, with the (433) structure shown in Fig. 4(*c*).

This procedure can be carried out between any two parent compounds shown in Fig. 2. To date most of these structures appear to be unknown, but one, the (332) structure shown in Fig. 4(*d*), which lies between Al_3Ti and Pt_2Mo, is adopted by Al_8Mo_3.[13]

The shift-lattice parameters of these structures are given in Table 2.

(h*k*0)-derived families of one-dimensional shift-lattice structures

All the phases constructed in the previous section had *g*-function boundaries on (210) planes. It is not difficult to generalise the method to any planes at all. In this section some of these phases are described and related to those above.

Table 2 Shift lattice parameters for the Au_4Mn (210) intermediate series of structures

formula	atom type	*w*	β
Au_4Mn	Mn	$0.5\alpha_1$	$2.5\alpha_1$
	Au	$2.0\alpha_1$	$2.5\alpha_1$
$Au_{22}Mn_6$	Mn	$0.5\alpha_1$	$2.333\alpha_1$
	Au	$1.833\alpha_1$	$2.333\alpha_1$
A_7B_2	B	$0.5\alpha_1$	$2.25\alpha_1$
	A	$1.75\alpha_1$	$2.25\alpha_1$
$A_{10}B_3$	B	$0.5\alpha_1$	$2.166\alpha_1$
	A	$1.666\alpha_1$	$2.166\alpha_1$
Al_8Mo_3	Mo	$0.5\alpha_1$	$1.833\alpha_1$
	Al	$1.333\alpha_1$	$1.833\alpha_1$

A phase of composition Au_3Mn with the Al_3Ti structure shown in Fig. 2(*b*) does not appear to exist in nature. However, a closely related Au_3Mn structure designated monoclinic I is known.[14] The structure is shown in Fig. 5(*a*). The structure is made up of an interleaved pair of shift-lattices, one containing the Mn atoms and the other containing just Au atoms. As well as the *g*-function boundaries, the sequence of Mn atoms along the *g*-function is also traced. (This makes the representation of these and particularly some of the following structures, easier to follow. However, large scale drawings reveal that the structures can be precisely delineated within *g*-functions, using the shift-lattice parameters given in Table 3.) The only significant difference between the Al_3Ti structure and Au_3Mn monoclinic I is that the *g*-function boundaries lie on (950), a rotation

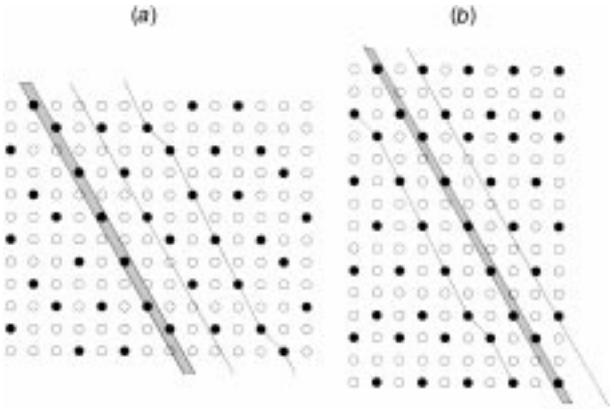

Fig. 5 The structures of (*a*) Au_3Mn monoclinic I, (*b*) $Ga_{13}Mn_5$. One Mn and one Au *g*-function is indicated and the sequence of Mn atoms along the Mn *g*-functions is indicated by the zigzag line.

Table 3 Shift lattice parameters for the (210)/(110) series of structures

formula	atom type	*g*-function	*w*	β
Al_3Ti	Ti	(210)	$0.5\alpha_1$	$2.0\alpha_1$
	Al	(210)	$1.5\alpha_1$	$2.0\alpha_1$
Au_3Mn(mon)	Mn	(950)	$0.45\alpha_1$	$2.222\alpha_1$
	Au	(950)	$1.555\alpha_1$	$2.222\alpha_1$
$Ga_{13}Nb_5$	Nb	(950)	$0.5\alpha_1$	$2.0\alpha_1$
	Ga	(950)	$1.5\alpha_1$	$2.0\alpha_1$
$Au_{53}Mn_{19}$	Mn	(32, 19, 0)	$0.4\alpha_1$	$2.25\alpha_1$
	Au	(32, 19, 0)	$1.18\alpha_1$	$2.25\alpha_1$
$Au_{35}Mn_{13}$	Mn	(21, 13, 0)	$0.35\alpha_1$	$2.286\alpha_1$
	Au	(21, 13, 0)	$1.936\alpha_1$	$2.286\alpha_1$
Au_5Mn_2	Mn	(320)	$0.56\alpha_1$	$2.333\alpha_1$
	Au	(320)	$1.772\alpha_1$	$2.333\alpha_1$
$Au_{43}Mn_{16}$	Mn	(750)	$0.55\alpha_1$	$2.4\alpha_1$
	Au	(750)	$1.90\alpha_1$	$2.40\alpha_1$
CuAu	Cu	(110)	$1.0\alpha_1$	$2.0\alpha_1$
	Au	(110)	$1.0\alpha_1$	$2.0\alpha_1$

of approximately 2.49° from the (210) planes used by Al_3Ti. The shift-lattice parameters are given in Table 3.

A homologous series of structures related to Au_3Mn monoclinic I could be generated by following the procedure set out in the previous section and varying the magnitude of the parameter β. The only member of this series so far located in the literature is $Ga_{13}Nb_5$.[15] The structure is shown in Fig. 5(*b*). It is differentiated from an Au_3Mn monoclinic I by a slightly smaller value of β.

Continued rotation of the *g*-function boundary will generate an enormous number of further structures. A small selection of these, which are known structures, are shown in Fig. 6. Each one of these structures can be made the parent of a homologous series if the values of the shift-lattice parameter β is changed.

The structure shown in Fig. 6(*a*) is that of $Au_{59}Mn_{19}$ monoclinic II.[16] In this structure the *g*-function boundaries are slightly nearer to (110) than the last two phases considered, and lie on (32, 19, 0). For clarity the *g*-function boundaries have been omitted and instead the sequence of Mn atoms along the *g*-function has been emphasised. This is quite complex. For ease of description the sequence can be thought of as made up of units of the (210)-type interspersed with units of the (110)-type, as shown in Fig. 6(*b*). Denoting these as 2 and 1 respectively, the repeat sequence along the *g*-function is [1222122122122122122]. The shift-lattice parameters for the construction of this phase are given in Table 3.

In the case of the closely related $Au_{35}Mn_{19}$ structure, shown in Fig. 6(*c*), the *g*-function boundary lies on (21, 13, 0).[17] The complex sequence of (210) and (110) units which comprise the Mn slab is [1221221212212], as shown in Fig. 6(*d*). The shift lattice parameters for both the Au and Mn lattices for these phases are contained in Table 3. Note that the rotation of the *g*-function boundaries between $Au_{59}Mn_{19}$ monoclinic II and $Au_{35}Mn_{19}$ is only 1.06°. This once again demonstrates that

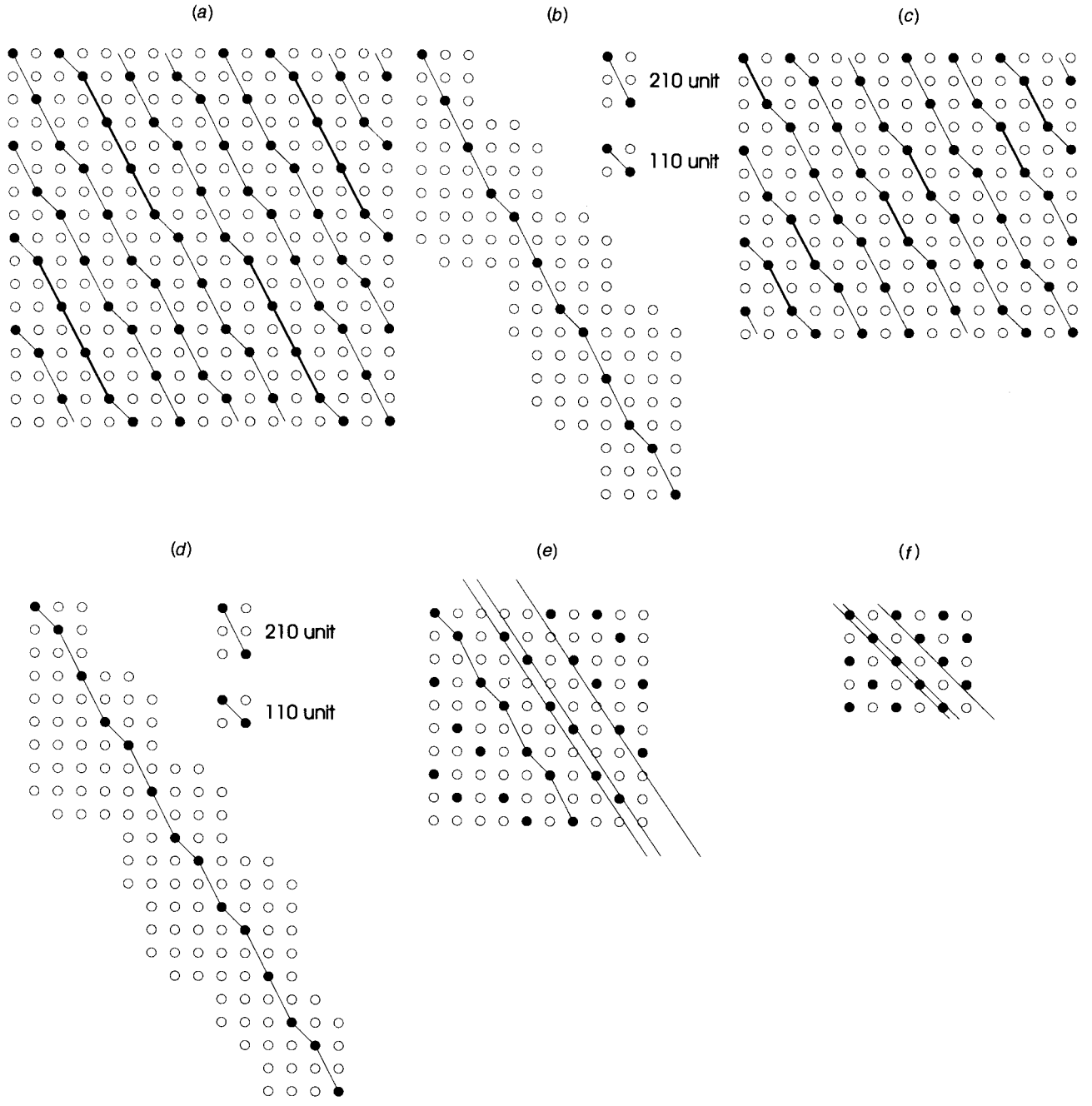

Fig. 6 (*a*) The structure of $Au_{53}Mn_{19}$ monoclinic I. (*b*) The complete sequence of Mn atoms along the Mn *g*-functions. (*c*) The structure of $Au_{35}Mn_{13}$. (*d*) The complete sequence of Mn atoms along the Mn *g*-functions. (*e*) The structure of Au_5Mn_2. (*f*) The structure of CuAu I. In (*a*) and (*b*), the Mn *g*-functions are not drawn for clarity. Au atoms are shown as open circles.

even the slightest change in shift-lattice parameters will produce quite different structures.

Although the phase Au_5Mn_2 has a simple formula, in shift-lattice terms it is neither more nor less complex than the two previous phases. The structure is shown in Fig. 6(*e*).[18] The *g*-function boundaries lie on (230); that confining the Mn atoms is shown. The other shift-lattice parameters are found in Table 3. Compared to the two previous structures, the sequence of 210 and 110 units lying along the *g*-function is rather simple.

To date we have not located any other structures which fall into the (210)/(110) series of one-dimensional shift-lattice phases, although the end member of the group, with *g*-function boundaries lying on (110), is the AuCu I structure, in the projection down the *c*-axis, as shown in Fig. 6(*f*).[9]

Gold microdomains

One of the more curious Au–Mn alloys has the composition $Au_{43}Mn_{16}$, shown in Fig. 7.[19] It is seen that the structure contains quite large coherently intergrown microdomains of Au, shown shaded. Despite the apparently uneven pattern of Mn distribution, this phase forms part of the continuum of phases discussed above. The structure can be constructed using *g*-function boundaries along (750) planes and the shift-lattice parameters given in Table 3. The microdomains are formed by the production of Mn planes of two types, shown as A and B in Fig. 7. The sequence in $Au_{43}Mn_{16}$ is [AAABBBB] and it is the juxtaposition of the set of A planes which produces the microdomains. By very small variations of the shift-lattice parameters, any number of A planes can be included, so as to create a wide variety of microdomain structures. It will be apparent from Fig. 7 that if the sequence of A planes is continued indefinitely, which is readily achieved by a small change of shift-lattice parameters, a structure results which is made up of alternating lamellae of Au-only regions and Au–Mn regions. This and other similar 'wallpaper' patterns have not been observed to date and so are not illustrated here.

Diffraction patterns

In general a one-dimensional shift-lattice in real space generates a shift-lattice-like array of diffraction spots in reciprocal space.[1,2] The diffraction pattern of a one-dimensional shift-lattice will consist of a row of 'superlattice' spots separated by β^* centred close to the nodes of the fcc α_1^* α_2^* reciprocal lattice and running at an angle normal to the *g*-function boundary in real space. In a structure made up of two one-dimension shift-lattices, the diffraction pattern of the structure can be constructed *via* the superposition of the diffraction patterns arising from the two components in real space.

In all of the one-dimensional shift lattices described above both the Au and the Mn components lie upon shift-lattices. In any one structure both shift-lattices have identical shift-lattice parameters except for the width of each *g*-function. The diffraction patterns of these phases will therefore be composed of two superimposed rows of superlattice reflections, each with the same spot spacing, equal to β^*. Thus the shift-lattice character of the structure will be retained in reciprocal space and displayed in the diffraction pattern.

This aspect is illustrated in the example shown in Fig. 8. The diffraction patterns from a set of atoms arranged at the positions equivalent to the Mn and Au portions of the structure of $Au_{22}Mn_6$ are shown separately in Fig. 8(*a*) and (*b*) respectively. The pattern shown in Fig. 8(*a*) consists of rows of superlattice spots of spacing β^* running normal to the *g*-function boundaries. The pattern due to the Au atoms, shown in Fig. 8(*b*), shows similar rows with the same spacing β^*, running in the same direction. However, these are not intense because the Au structure is almost a complete fcc array with only a small number of 'vacancies' present corresponding to the Mn positions. This tends to diminish the shift-lattice contribution with respect to the fcc sub-cell reflections, which are prominent in Fig. 8(*b*). Despite this, the resultant patterns made from the sum of both of these contributions still clearly reveals shift-lattice-like features.

Discussion

The one-dimensional shift-lattice formalism has been shown to be an efficient method of generating large numbers of commensurate and semi-commensurate structures. All of the binary Au_4Mn-related fcc substituted alloy phases that have been found in the literature have been shown to have both atomic components shift-lattice distributed in the structure. Because the important shift-lattice parameters, α and β, are identical for each of these shift-lattices, the shift-lattice nature of the structure is retained and displayed in the diffraction patterns of these phases.

The pattern of structures described in Fig. 5, 6 and 7 can be seen in the light of the concept of 'swinging shear planes' described by Hyde and Andersson.[20] A vast number of phases can be generated simply by rotating the *g*-function boundaries and creating a homologous series on the resultant structure formed. These and all of the other structures described in this paper can be described as 'ordered intergrowths'. Although there is some convenience in this description it is cumbersome compared to the much simpler shift-lattice description which

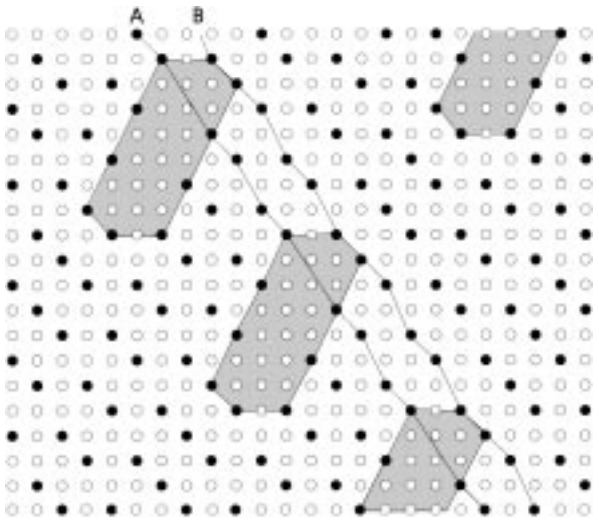

Fig. 7 The structure of $Au_{43}Mn_{16}$. The zigzag lines show the sequence of Mn atoms along the Mn *g*-functions, which are not drawn. The shaded regions show microdomains of Au.

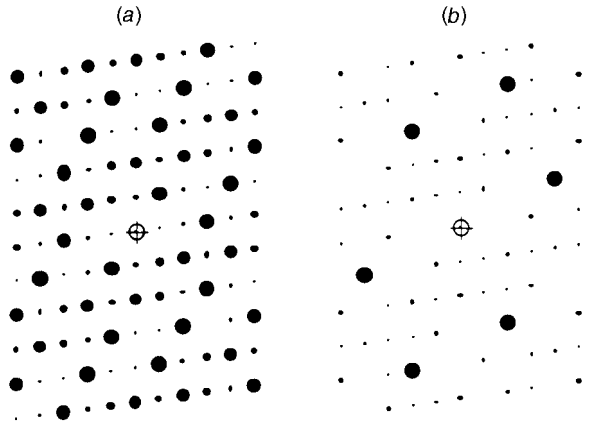

Fig. 8 (*a*) The diffraction pattern from the Mn-only portion and (*b*) the Au-only portion of the $Au_{22}Mn_6$ structure

includes not only the phases described but many other 'wall-paper' structures as well. Moreover, the intergrowth description obscures the fact that both of the metal atom arrays are shift-lattices.

In conclusion, the use of the shift-lattice formalism has allowed a large number of diverse alloy structures to be correlated and the shift-lattice nature of their diffraction patterns explained.

References

1 G. Harburn, R. J. D. Tilley, J. M. Williams and R. P. Williams. *Nature* (*London*), 1991, 350.
2 G. Harburn, R. J. D. Tilley, J. M. Williams and R. P. Williams, *Proc. R. Soc. London, Ser. A*, 1993, **440**, 23.
3 R. J. D. Tilley and R. P. Williams, *Philos Mag*., 1994, **69**, 151.
4 G. Harburn, B. H. Parry, R. J. D. Tilley and R. P. Williams, *Aust. J. Chem*., 1992, **45**, 1397.
5 R. J. D. Tilley and R. P. Williams, *Acta Crystallogr., Sect. B*, 1995, **51**, 758.
6 M. M. Moore, R. J. D. Tilley and R. P. Williams, *Proc. R. Soc. London, Ser. A*, 1996, **452**, 841.
7 R. J. D. Tilley and R. P. Williams, *Z. Kristallogr*., 1995, **210**, 81.
8 R. J. D. Tilley and R. P. Williams, *Aust. J. Chem*., 1996, **49**, 873.
9 See *e.g.* W. B. Pearson, *The crystal chemistry and physics of metals and alloys*, Wiley Interscience, New York, 1972.
10 P. Norby and A. N. Christensen, *Acta Chem. Scand. A*, 1986, **40**, 157.
11 H. Ocken and J. H. N. van Vucht, *J. Less Common Met*., 1968, **15**, 193.
12 K. Hiraga, M. Hirabayashi, O. Terasaki and D. Watanabe, *Acta Crystallogr., Sect. A*, 1982, **38**, 269.
13 J. B. Forsyth and G. Gran, *Acta Crystallogr*., 1962, **15**, 100.
14 G. van Tendeloo, R. Wolf, J. van Landuyt and S. Amelinckx, *Phys. Status Solidi A*, 1978, **47**, 539.
15 H-G. Meissner and K. Schubert, *Z. Metallk*., 1965, **56**, 475.
16 R. Wolf, G. van Tendeloo, J. van Landuyt and S. Amelinckx, *Phys. Status Solidi A*, 1978, **48**, 39.
17 G. van Tendeloo and S. Amelinckx, *Phys. Status Solidi A*, 1982, **71**, 185.
18 S. G. Humble, *Acta Crystallogr*., 1964, **17**, 1485.
19 G. van Tendeloo and S. Amelinckx, *Phys. Status Solidi A*, 1984, **84**, 185.
20 B. G. Hyde and S. Andersson, *Inorganic Crystal Structures*, Wiley Interscience, Chichester, 1989, pp. 99–104.

Paper 7/06549C; *Received* 8*th September*, 1997